Resonant inelastic x-ray scattering probes the electron-phonon coupling in the spin liquid κ-(BEDT-TTF)$_2$Cu$_2$(CN)$_3$

V. Ilakovac,[1,2,*] S. Carniato,[1] P. Foury-Leylekian,[3] S. Tomić,[4] J.-P. Pouget,[3] P. Lazić,[5] Y. Joly,[6] K. Miyagawa,[7] K. Kanoda,[7] and A. Nicolaou[8]

[1]*Sorbonne Universités, UPMC, Université Paris 6, CNRS UMR 7614, Laboratoire de Chimie Physique–Matière et Rayonnement, Paris, France*

[2]*Université de Cergy Pontoise, Département de Physique, F-95031 Cergy-Pontoise, France*

[3]*Laboratoire de Physique de Solides, CNRS UMR 8502, Université Paris Sud, Université Paris Saclay, Orsay, France*

[4]*Institut za fiziku Bijenička cesta 46, HR-10000 Zagreb, Croatia*

[5]*Ruder Bošković Institute, Bijenička cesta 54, HR-10000 Zagreb, Croatia*

[6]*Univ. Grenoble Alpes, CNRS, Grenoble INP, Institut Néel, 38042 Grenoble, France*

[7]*Department of Applied Physics, University of Tokyo, Tokyo 113-8656, Japan*

[8]*Synchrotron SOLEIL, L'Orme des Merisiers, Saint-Aubin, Boîte Postale 48, F-91192 Gif-sur-Yvette, France*

(Received 27 July 2017; published 17 November 2017)

Resonant inelastic x-ray scattering at the N K edge reveals clearly resolved harmonics of the anion plane vibrations in the κ-(BEDT-TTF)$_2$Cu$_2$(CN)$_3$ spin-liquid insulator. Tuning the incoming light energy at the K edge of two distinct N sites permits us to excite different sets of phonon modes. The cyanide (CN) stretching mode is selected at the edge of the ordered N sites which are more strongly connected to the bis(ethylenedithio)tetrathiafulvalene (BEDT-TTF) molecules, while positionally disordered N sites show multimode excitation. Combining measurements with calculations on an anion plane cluster permits us to estimate the site-dependent electron-phonon coupling of the modes related to nitrogen excitation.

DOI: 10.1103/PhysRevB.96.184303

I. INTRODUCTION

Electron-phonon coupling (EPC) plays a fundamental role in many aspects of condensed-matter physics. It governs the charge mobility and optical properties in metals and semiconductors, it drives the Peierls metal-insulator instability in charge density wave compounds, and it gives rise to the conventional superconductivity [1], while its role in unconventional superconductivity is under persisting debate. Among experimental techniques permitting us to measure the EPC strength, like IR, Raman, angle-resolved photoemission spectroscopy, inelastic neutron scattering, and, more recently, ultrafast transient response of the optical reflectivity [2], none of them is at the same time element selective, site dependent, and momentum resolved like resonant x-ray scattering (RIXS). In the last decade improvement of the resolving power of RIXS spectrometers, going up to $E/\Delta E$ of 2.5×10^4 [3], has made it an excellent technique for the direct measurement of the EPC strength with all these advantages.

Understanding how the lattice dynamics couples to charge and spin degrees of freedom in κ-(BEDT-TTF)$_2$Cu$_2$(CN)$_3$ (k-ET-Cu for short) is of primary importance for its spin-liquid [4] and pressure-induced superconducting properties [5–7]. This charge-transfer salt is composed of two alternating building blocks, as shown in Fig. 1(a). One is the donor layer of triangular constellations of dimers of ET [BEDT-TTF, bis(ethylenedithio)tetrathiafulvalene] molecules. The other is the anion plane, consisting of triangularly coordinated Copper(I) ions linked by cyanide (CN) groups [5]. The two are connected via the C–H–N hydrogen bond. Each dimer donates approximately one electron to the anion plane, creating a triangular lattice of holes with spin-1/2. The absence of spin ordering despite an exchange coupling of $J \approx 250$ K was explained by the total frustration of spins on this triangular lattice [4]. But more recent *ab initio* calculations pointed to slightly anisotropic transfer integrals between dimers [8,9], which raised the question of the origin of the spin-liquid state. A possible explanation lies in an interaction between spins and charge dynamics [10,11] and spinon-phonon interaction, as pointed out by the ultrasonic wave measurements [12]. Finally, the actual debate about the role of phonons in the Cooper pairing applies perfectly to its pressure-induced unconventional superconductivity [13].

There is much evidence of the strong dynamic and/or static disorder in k-ET-Cu. An inherent disorder is present already in the conventional $P2_1/c$ structure as one third of the anion plane CN groups lies on an inversion point and is thus orientationally disordered [see Fig. 1(b)]. Moreover, ET-ethylene end groups can take different conformations relative to the rest of the molecule, similar to other (ET)$_2X$ compounds [14,15]. Ethylene hydrogen atoms form stronger H bonding with nitrogen atoms in ordered polymeric chains (N_C), compared to disordered bridging sites (N_B). A subtle interaction between electrons and lattice vibrations is observed in conducting and dielectric properties. The dc conductivity shows an insulating behavior, described by nearest-neighbor hopping at ambient temperature and variable-range hopping below $\approx$ 130 K, while below 50 K, Hall measurements indicate a complete freezing of charge carriers [16,17]. Although there are no electric dipoles associated with the ET dimers [18], the fingerprints of relaxor ferroelectricity have been established by dielectric spectroscopy below 60 K [16,19].

In this work, we focus on the anion plane dynamics as this part of the system controls the donor packing and is an intrinsic source of disorder. We show that N K-edge RIXS

*vita.ilakovac-casses@upmc.fr

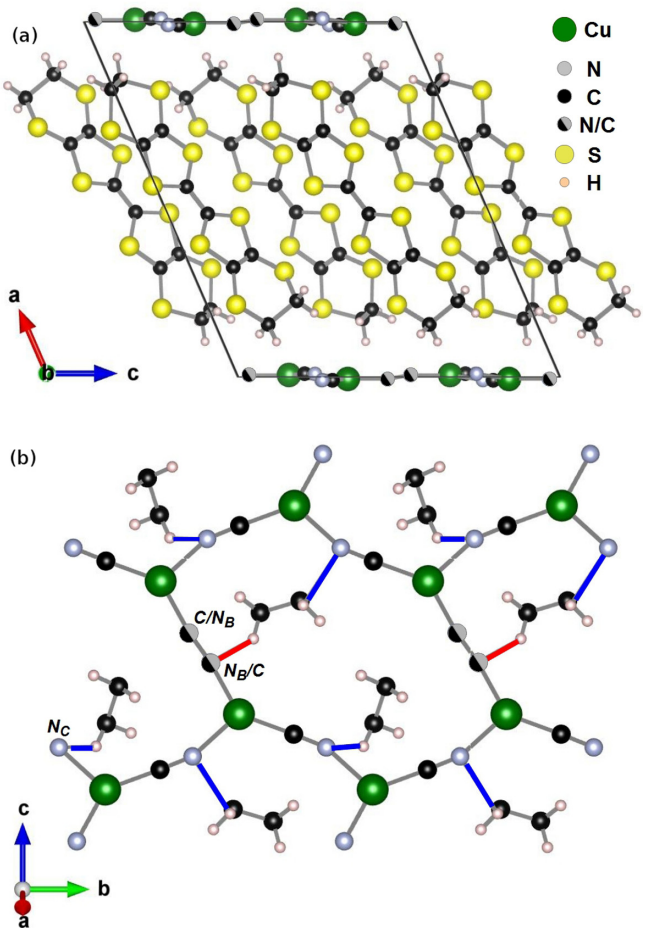

FIG. 1. (a) k-ET-Cu structure seen along the b axis. (b) $Cu_2(CN)_3$ anion plane with Cu-CN_C-Cu polymeric chains and bridging, orientationally disordered CN_B groups. Blue lines indicate HN_C bonds (2.72–2.79 Å), and red lines show HN_B bonds (2.80 Å) connecting to ethylene end groups of ET molecules just below.

permits us to switch on two different dynamics related to nonequivalent nitrogen sites which are differently coupled to the ET molecular layer. One of these sites shows an essentially monomode excitation with five clearly resolved harmonics which show up in RIXS spectra. Despite the complexity of the system, our RIXS calculations, performed on an anion plane cluster and including vibrational progression, describe well the experimental spectra and permit us to determine the electron-phonon coupling of the selected phonon modes.

II. EXPERIMENTAL AND CALCULATION DETAILS

A high-quality single-crystal sample of k-ET-Cu was grown using the electrocrystallization method [5,6]. N K-edge (≈400 eV) RIXS measurements were acquired at the SEXTANTS beamline (synchrotron SOLEIL) [20,21] with an overall energy resolution of 115 meV. Near-edge x-ray absorption spectroscopy (NEXAFS) measurements were performed in the total electron yield mode with the beamline resolution set to 80 meV. Data were recorded in grazing incidence geometry (see the inset of Fig. 3 below), with the incoming photon polarization ε almost perpendicular to the anion layer

TABLE I. Anion layer interatomic distances (in Å) and angles (in degrees) in the conventional crystal $P2_1/c$ structure [5]. They are compared to equivalent distances and angles in the initial- and excited-state cluster $Cu_2(CN)_5H_4$ used for RIXS calculation.

	CN	CuN	CuC	CuCu	∠CuNC	∠CuCN
Crystal						
Chain	1.130	2.026	1.872	4.933	158.9	177.3
Bridge	1.188	1.895	1.895	4.962	169.4	169.4
Cluster						
Initial state	1.156	1.928	1.931	5.013	176.2	178.8
Excited state	1.195	1.991	1.845	5.026	176.1	178.9

$\angle(\varepsilon,a^*) = 20°$, or $\varepsilon \perp a^*$, where a^* stands for the reciprocal lattice vector perpendicular to the (b,c) plane. The orientation of the b and c axes with respect to the scattering plane was not determined. The sample was measured as introduced in a temperature range from 300 to 25 K. NEXAFS calculations were performed with the Finite Difference Method Near Edge Structure (FDMNES) code [22,23] using coordinates of the conventional $P2_1/c$ structure [5]. RIXS calculations were performed on a five-cyanide cluster cut from the anion plane, $Cu_2(CN)_5H_4$. Its four peripheral cyanide groups were ended by hydrogen atoms in order to ensure the chemical stability, while the central cyanide nitrogen atom was core excited. Frequencies of the normal modes and the geometry optimization in the initial and intermediate states of the RIXS process were calculated by density-functional theory (DFT) using the GAMESS(US) program [24]. For the quasielastic part of the spectra, the calculation of Franck-Condon amplitudes was performed with the method using the frequencies of the initial and final states and taking into account the deformation of the cluster from the initial state to the intermediate state [25]. For the inelastic part of the spectra, the linear-coupling method was applied, where the initial- and intermediate-state potentials are supposed to be harmonic and of the same frequency.

III. NEXAFS SPECTRA REVEAL TWO DISTINCT NITROGEN SITES

The low-temperature N K-edge NEXAFS spectrum of the single crystal of k-ET-Cu is shown in Fig. 2. It has a prominent structure at a photon energy of $h\nu = 399.8$ eV and a low-energy shoulder at about $h\nu = 398.4$ eV. In order to identify these two features, we performed calculation using the FDMNES code for the two types of N sites (N_B, N_C) and for two orientations of the incident light polarization, parallel and perpendicular to a^*. The shapes of N_B and N_C spectra are very different because the local environment of these two nonequivalent sites is not the same. For the same reason they also present a relative core-level shift, higher for N_C compared to N_B. Indeed, the cation-ET-molecular layer imposes constraints on the anion plane, resulting in an elongation of the bridging Cu-CN_B-Cu and a compression and bending of the chain Cu-CN_C-Cu links (see Table I). The negative shift of the N_B feature of $\Delta E \approx 2.5$ eV compared to the main N_C structure is, however, overestimated compared to the experimental value of ≈1.5 eV. The reason for this

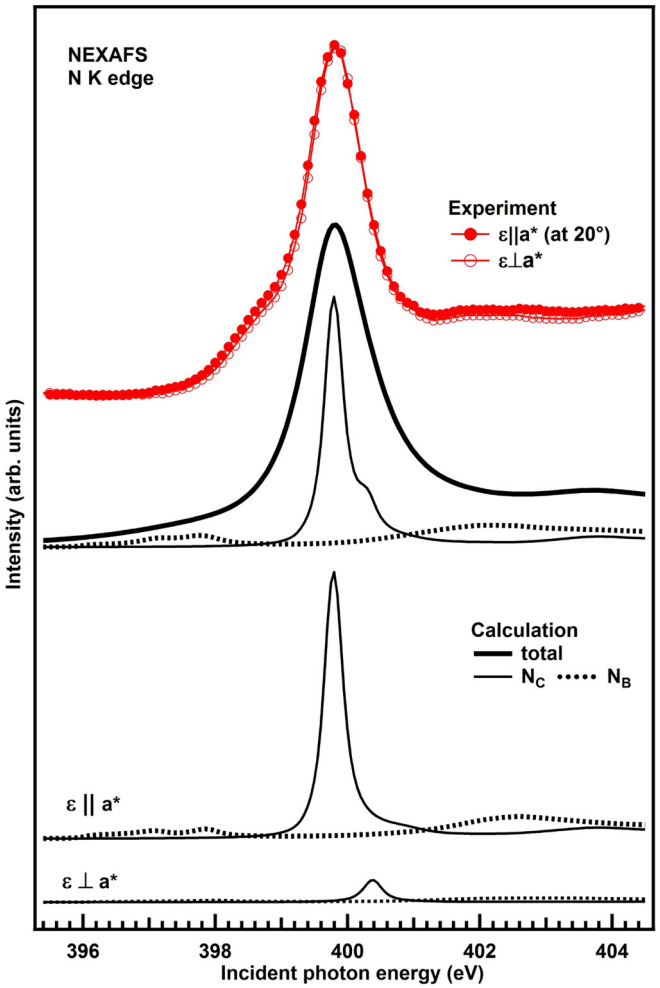

FIG. 2. NEXAFS spectra (red circles) measured for $\angle(\varepsilon,a^*) = 20^\circ$ and $\varepsilon \perp a^*$ showing negligible polarization dependence. Calculated spectra (thick black line) are performed for $\angle(\varepsilon,a^*) = 20^\circ$ and enlarged to take into account the dynamics of the system. Contributions of N_C/N_B sites are shown without enlargement. The $\varepsilon \parallel a^*$ and $\varepsilon \perp a^*$ contributions of N_C/N_B sites are shown below.

discrepancy is the description of the orientational disorder of bridging CN_B cyanide groups in the conventional $P2_1/c$ structure [5]. In this structure, CN_B groups are centered at inversion points. The CN_B distance is determined as the distance between statistical positions of C/N_B and N_B/C atoms and is unnaturally increased. Moreover, the symmetry imposes equal Cu-C and Cu-N_B distances for a cyanide CN_B. On the other hand, in the case of chain Cu-CN_C-Cu links, the carbon is closer to its copper neighbor, and the CN_C distance is shorter.

Further, the linear dichroism of the k-ET-Cu NEXAFS is surprisingly negligible; that is, there is almost no polarization dependence when comparing spectra with $\angle(\varepsilon,a^*) = 20^\circ$ and $\varepsilon \perp a^*$ [$\varepsilon \parallel$ to (b,c) plane], as shown in Fig. 2. However, NEXAFS spectra of a similar system, planar nitrile molecules, show two prominent white lines, corresponding to excitations to $\pi^*_\perp$ and $\pi^*_\parallel$ states, with symbols $\perp$ and $\parallel$ meaning relative to the molecular plane. Their relative shift of about 1 eV is explained by a conjugation interaction inside the linear

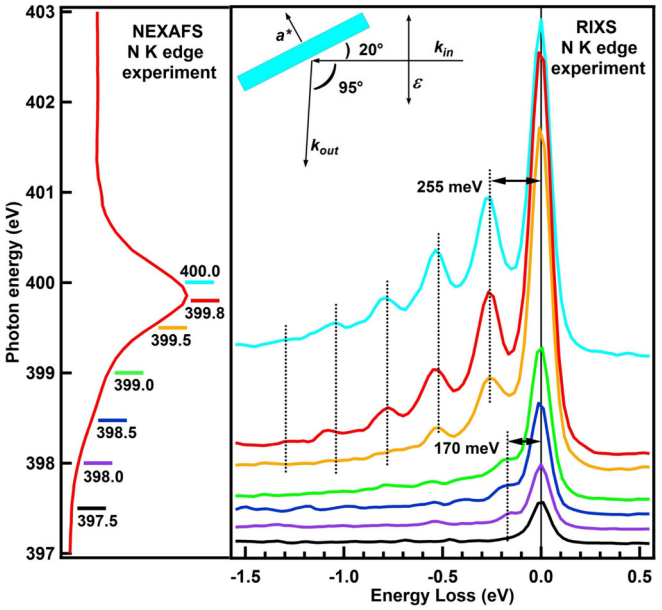

FIG. 3. Low-temperature NEXAFS (60 K, left) and RIXS (25 K, right) spectra, shifted for clarity. The inset shows the experimental geometry, with the polarization vector ε in the scattering plane.

arrangement of C=C and C ≡ N bonds [26–29]. Linear C=C–C ≡ N geometry and a strictly planar system are therefore two conditions for splitting $\pi^*_\perp$ and $\pi^*_\parallel$, which are nominally degenerate. In FDMNES calculations of the k-ET-Cu spectrum, N_C spectra projected to the $\pi^*_\perp$ and $\pi^*_\parallel$ states, with $\perp$ and $\parallel$ meaning relative to the anion plane, are separated by only 0.5 eV. The conjugation effect is here decreased already by the 30° deviation from the linear arrangement of the Cu–CN_C–Cu bonds. The residual disagreement between the experiment and the FDMNES calculations in terms of the polarization dependence can be explained by the DFT approach. It does not describe correctly the effect of hydrogen bonding between the anion layer nitrogen and ethylene end group hydrogen atom. Note that this effect should be stronger for N_C (H-N_C = 2.72–2.79 Å) compared to N_B (H-N_B = 2.80 Å).

We stress the fact that even if the match between the experimental and the calculated NEXAFS spectra is not perfect, comparing them permits us to identify the NEXAFS main peak related to the N_C sites and the low-energy shoulder related to the N_B sites.

IV. SITE-DEPENDENT LATTICE MOTION FINGERPRINTS IN THE QUASIELASTIC PART OF THE RIXS SPECTRA

Low-temperature N K-edge RIXS spectra are shown in Fig. 3. The experimental geometry is indicated in the inset. RIXS spectra were collected at photon energies indicated on the NEXAFS spectrum by the line of the same color. For incoming photon energies above $h\nu = 397.5$ eV, the elastic peak develops an asymmetric tail, which transforms into a clear vibrational progression, which directly concerns nitrogen sites of the anion CN groups. A recent detailed study of the k-ET-Cu lattice vibrations [30] reported that there are essentially three distinct families of modes affecting the CN groups. Their

TABLE II. The most important vibrational modes involving anion CN groups (see Fig. 4). Cluster calculation wave numbers σ (in cm^{-1}) and energy quanta $\hbar\omega$ (in meV) are compared to those in the crystal [30]. Corresponding values of Huang-Rhys parameters S, gradients in dimensionless normal coordinates g (in meV), and dimensionless EPC λ are given with their relative errors in parentheses [31].

Mode	CN stretching	CN sliding	CN bending
n	1	2	3
Crystal [30]	k-ET-Cu		
σ	2100–2140	508–515	195–225
$\hbar\omega$	260–265	63–64	24–28
Cluster	$Cu_2(CN)_5H_4$	calculations	
σ_n (6%)	2258	510	200
$\hbar\omega_n$ (6%)	280	64	25
S_n (6%)	0.334	0.608	0.235
g_n (9%)	230	71	17
λ_n (35%)	0.076	0.032	0.004

energy quanta will be designated by $\hbar\omega_n$, with $n = 1,2,3$. They are identified as CN stretching ($\hbar\omega_1 = 260$–265 meV), CN sliding between Cu atoms ($\hbar\omega_2 = 60$–65 meV), and low-energy modes combining CN bending, stretching, and twisting ($\hbar\omega_3 = 8$–50 meV), as presented in Table II. The vibrational progression at $h\nu = 399.5$–400.0 eV shows distinct and perfectly resolved harmonics, separated by 255 meV, indicated by equidistant dotted lines. They are attributed to CN stretching motion ($\hbar\omega_1$). Below the NEXAFS maximum, in the range $h\nu = 398$–399 eV (NEXAFS shoulder), an energy loss of 170 meV is revealed (see Fig. 3, right). Its energy does not correspond to any simple CN group movement and points rather to a multimode excitation.

In order to reproduce these experimental data we have performed RIXS calculations using the $Cu_2(CN)_5H_4$ cluster depicted in Fig. 4. It was chosen because its interatomic distances and normal-mode frequencies match well reported values in the k-ET-Cu crystal [5,30] (see Tables I and II). However, it does not include effects of the ET cation layer. The cluster has a naturally linear Cu-CN-Cu arrangement characteristic of the C ≡ N bond, while in the real crystal, stronger H bonding of ethylene end groups to the N_C sites drags nitrogen in polymeric chains and deforms (bends) Cu-CN_C-Cu links [see Fig. 1(b)]. For Cu-CN_B-Cu bridging sites this deformation is much smaller.

Considering the grazing-incidence geometry explored in the experiment (see the inset of Fig. 3), we considered that in the intermediate state the core electron is accommodated

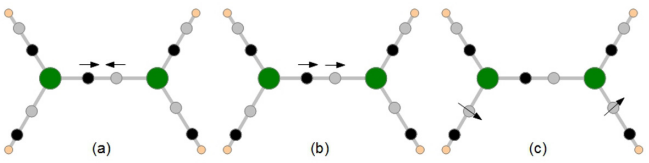

FIG. 4. $Cu_2(CN)_5H_4$ cluster used for RIXS calculations and its most important normal modes: (a) CN stretching $\hbar\omega_1$, (b) CN sliding $\hbar\omega_2$, and (c) CN bending $\hbar\omega_3$.

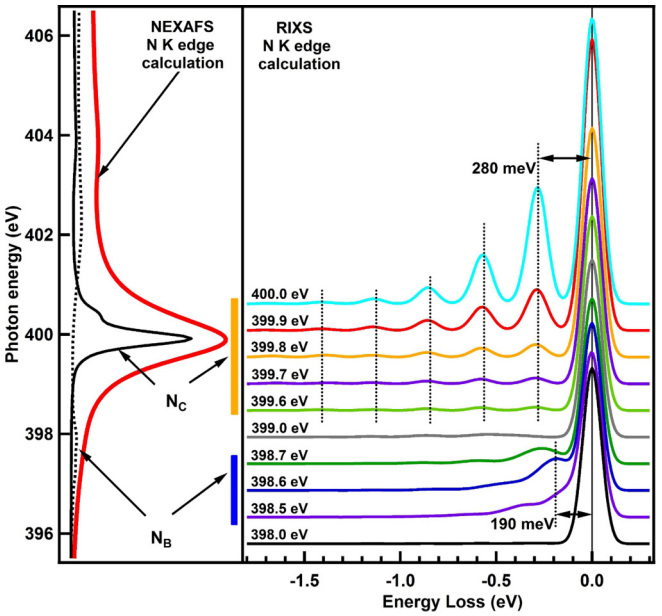

FIG. 5. Left: NEXAFS calculation (red line) and N_C and N_B contributions. Right: RIXS calculation on a $Cu_2(CN)_5H_4$ anion plane cluster.

in the $\pi^*_\perp$ orbital system (perpendicular to the anion plane), while the initial and final electronic states are the same. The calculated value of the $1s \rightarrow \pi^*_\perp$ transition of the $Cu_2(CN)_5H_4$ cluster is 398.6.0 eV, considered to be the resonance of the N_B sites. The resonance of the N_C sites was set to 1.5 eV higher energy, corresponding to the energy difference between the two distinct behaviors observed in the RIXS experiment. In terms of phonon excitation, the final state differs strongly from the initial situation even if only a few modes are relevant for the description of the quasielastic part of the spectra: CN stretching ($\hbar\omega_1$), CN sliding ($\hbar\omega_2$), and CN bending ($\hbar\omega_3$), depicted in Fig. 4.

In order to compare experimental data with calculations, calculated NEXAFS and RIXS spectra are shown in Fig. 5 in the same manner as the experimental results in Fig. 3. The RIXS calculation shows that the resonant behavior of the vibrational progression calculated using this simple cluster model agrees well with the experiment.

When the RIXS calculation is performed for photon energy $h\nu = 398.6$ eV, corresponding to the resonance of the N_B sites (NEXAFS shoulder), three normal modes are strongly excited. The left panel of Fig. 6 shows the monomode contributions of the three modes ($n = 1$–3), the elastic peak (Thomson scattering), and how they all interfere in the RIXS spectra (labeled "all"). On the other hand, the calculation with the photon energy set to $h\nu = 400$ eV (N_C sites, NEXAFS main peak), shown in the right panel of Fig. 6, matches the experiment when solely CN stretching ($\hbar\omega_1$) is included. Clearly, real-crystal constraints in the curved Cu-CN_C-Cu conformation prevent strong excitation of any other motion related to the CN_C group. Strong excitation of any other mode would indeed completely destroy the CN stretching vibrational progression with distinct harmonics, similar to the case of the N_B excited sites in the left panel of Fig. 6. Moreover, Cu-N

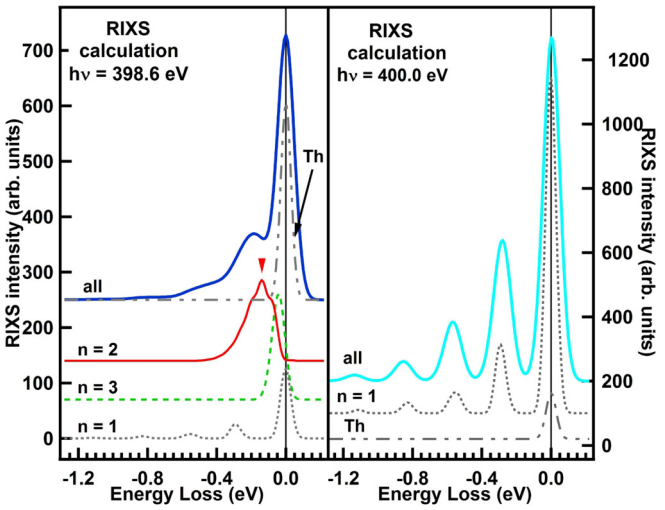

FIG. 6. RIXS spectra calculated for $h\nu = 398.6$ eV (N_B sites, NEXAFS shoulder) and $h\nu = 400.0$ eV (N_C sites, NEXAFS main peak). Each spectrum is decomposed in its monomode contributions ($n = 1$–3) and the Thompson scattering (Th). For $h\nu = 398.6$ eV the second most excited harmonic of the CN sliding motion ($n = 2$) is indicated by an arrow. Note that the "all" spectra include interference effects and experimental resolution broadening.

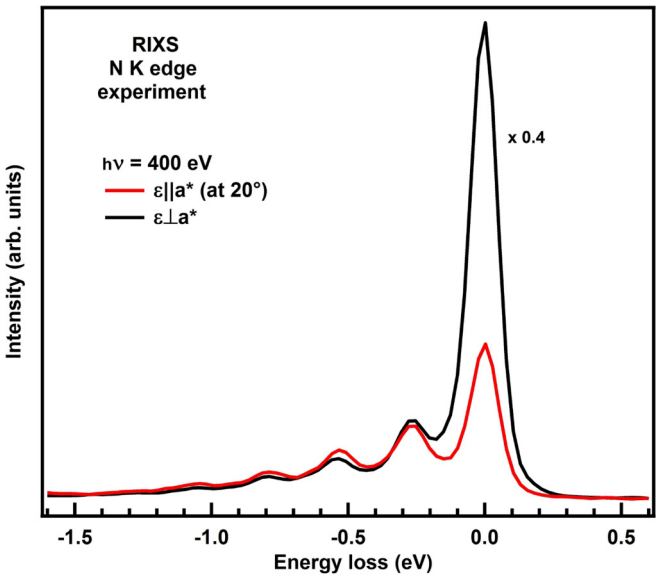

FIG. 7. Experimental RIXS spectra measured at $h\nu = 400$ eV for two orientations of the incident electric field, $\angle(\varepsilon, a^*) = 20^\circ$ and $\varepsilon \perp a^*$. In order to better compare the two vibrational progressions, the intensity of the $\varepsilon \perp a^*$ spectrum is multiplied by 0.4.

and Cu-C distances in the real crystal are already close to those of the N K-edge excited-state cluster. Small excited-state cluster deformation relative to the real crystal Cu-CN_C-Cu conformation explains the lack of vibrational modes besides the highest-energy CN stretching. Weak excitation of low-energy modes is, however, not excluded and should contribute to the tail of the elastic peak observed in the experiment. Finally, changing the polarization to $\varepsilon \perp a^*$ does not change the vibrational progression, only the intensity of the elastic peak (see Fig. 7).

The observed resonant modification of the vibrational progression in the quasielastic part of the N K-edge RIXS spectra confirms that the NEXAFS main peak and the NEXAFS shoulder are related to two different nitrogen sites, N_C and N_B, respectively. With the help of RIXS calculations, we determine that the CN_C groups are restricted to almost monomode motion, while CN_B groups show at least three strongly excited modes.

V. INELASTIC PART OF THE RIXS SPECTRA: CHARGE-TRANSFER EXCITATIONS

Large-energy-range RIXS spectra are shown in Fig. 8. They are presented in the emitted-energy scale in order to point out the almost non-Raman behavior of inelastic features A and B. Feature A appears at slightly lower incident photon energy $h\nu$ and has almost constant intensity in a range of about 2 eV, while feature B resonates at $h\nu = 399.8$ eV, corresponding to the NEXAFS maximum. The emitted photon energies of their maxima are $h\nu' \approx 394.5$ eV and $\approx$392.0 eV, respectively.

RIXS calculations are performed on the $Cu_2(CN)_5H_4$ cluster (see Fig. 9), like for the quasielastic part. Structure A is identified as the excitation of an N 1s electron to the first unoccupied orbital ($\pi^*_\perp$) followed by the $\pi_\perp$, $\pi_\parallel \rightarrow$ N 1s decay, giving rise to $h\nu_{A1}$, $h\nu_{A2}$ emissions, respectively, as schematized in Fig. 10(a). In terms of initial and final states, it is thus a signature of two transitions: $\pi_\perp \rightarrow \pi^*_\perp$ and $\pi_\parallel \rightarrow \pi^*_\perp$. The $\pi_\perp \rightarrow \pi^*_\perp$ transition is potentially related to the ET cation $\rightarrow$ anion charge transfer, which is not described in the present anion-cluster calculations. The $\pi_\parallel \rightarrow \pi^*_\perp$ transition is a charge transfer from an orbital which is delocalized on three neighboring cyanide groups to a $\pi^*_\perp$ orbital, which is localized mostly on the carbon atom of the central (excited) cyanide

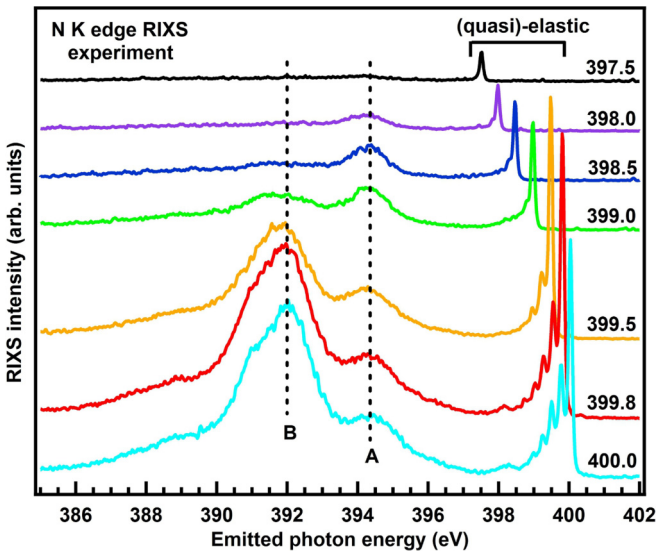

FIG. 8. Emitted-energy scale $h\nu'$ RIXS spectra measured at 25 K. The corresponding incident photon energy $h\nu$ is given on the right side of each spectrum. Dashed lines indicate the emitted energy of the positions of structures A and B at the NEXAFS maximum ($h\nu = 399.8$ eV).

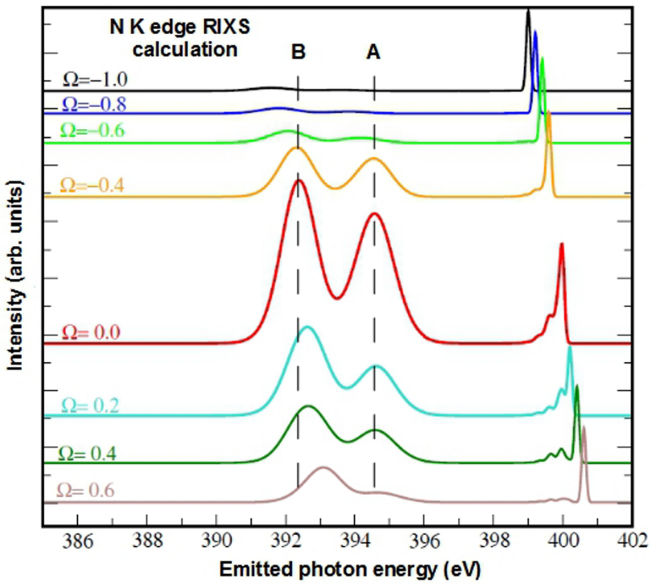

FIG. 9. Calculation of the RIXS spectra including inelastic events. The detuning energy Ω (in eV), relative to the NEXAFS maximum, is indicated for each spectrum. Dashed lines indicate the positions of structures A and B for $\Omega = 0$.

group. The former is possibly related to the effective EPC including the ET molecular layer, while the latter is connected to the intra-anion-plane electron-phonon interaction. Similarly, structure B, with lower emitted energy $h\nu_B$, can be described as the $\sigma \rightarrow \pi_\perp^*$ transition [see Fig. 10(b)].

As the $Cu_2(CN)_5H_4$ cluster is a system with discrete energy levels, features A and B are supposed to show Raman behavior, i.e., shift in the emitted photon energy $h\nu'$ scale, in the same manner as the elastic peak. This shift is indeed present in the

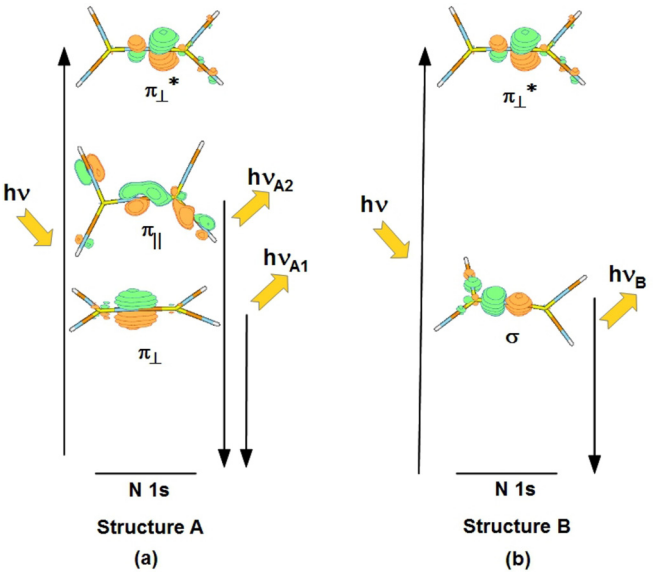

FIG. 10. Inelastic RIXS processes giving rise to structures A and B, with emitted photon energy $h\nu' = h\nu_{A1}$, $h\nu_{A2}$, and $h\nu_B$. Lobes of the $\pi_\perp$, $\pi_\parallel$, and σ orbitals are presented in the initial state; those of the $\pi_\perp^*$ orbital are presented in the excited state.

calculated spectra in Fig. 9 for incident photon energies $h\nu$ away from the resonance. When the dynamics of the system is included via vibrational-progression calculations, the position of features A and B remains constant when approaching the resonance ($h\nu \approx 399.8$ eV). Similar constant emitted-energy resonant behavior is observed in RIXS spectra of a very small system such as the HCl molecule [32]. Thus, even for small systems, strong EPC induces non-Raman behavior in RIXS spectra.

In the inelastic part of the N K-edge RIXS spectra three charge-transfer excitations are identified: $\pi_\perp \rightarrow \pi_\perp^*$ and $\pi_\parallel \rightarrow \pi_\perp^*$ closer to the elastic peak and $\sigma \rightarrow \pi_\perp^*$, with about 2 eV lower emitted energy. Cluster calculation including dynamics shows that their Raman behavior is suppressed at resonance.

VI. EXTRACTING THE ELECTRON-PHONON COUPLING FROM THE RIXS SPECTRA

The theoretical work of Ament *et al.* [33] indicates how the EPC can be estimated from the envelope of the RIXS spectra vibrational progression. In the case of localized Einstein phonon modes, a simple expression is derived under ultrashort core-hole lifetime approximation ($\Gamma \gg \hbar\omega$). It relates EPC to the relative intensity of the first and the second harmonics, the core-hole lifetime broadening Γ, and the phonon quantum $\hbar\omega$. In this way, EPC of selected phonon modes was extracted from the Ti L-edge RIXS spectra of titanates [34,35]. For the edge we are dealing with, this approximation is not valid, as both values of Γ reported in the literature, 93 meV [36] and 132 meV [36,37], are lower than $\hbar\omega_1 = 250$ meV.

Alternatively, the EPC of a selected mode n can be derived from our $Cu_2(CN)_5H_4$ cluster calculations. The demonstration will be performed using the linear-coupling model, where the potentials in the initial and the excited states are supposed to be harmonic and have the same frequency ω_n. The excited state is here a state with a core hole and a supplementary electron in the valence band. Figure 11 shows the two electronic-state potentials with corresponding vibrational wave functions. The phonon coupling to this electronic excitation is evaluated by the overlap of the initial state and the excited-state wave functions. The excited state is shifted relative to the initial state for a value of δq_n in normal coordinates. For small δq_n, the overlap of the initial- and excited-state fundamentals prevails, and the vibronic excitation is small. But, as δq_n increases, higher harmonics of the excited state have a stronger overlap with the initial-state wave function, leading to a stronger vibronic coupling. The Huang-Rhys (HR) parameter [38] evaluates overlaps of wave functions of the two harmonic potentials. It is calculated from the normal-mode coordinate shift δq_n of the two potentials and their frequency:

$$S_n = \frac{\omega_n}{2\hbar}\delta q_n^2 \tag{1}$$

For the quasielastic part of the spectra, δq_n is calculated by taking into account the deformation of the cluster from the initial to the intermediate state [25]. Nevertheless, the derivation of the EPC parameter is more evident when δq_n is calculated from the gradient of the excited-state potential at $q_n = 0$ (green line in Fig. 11), as was done for the inelastic

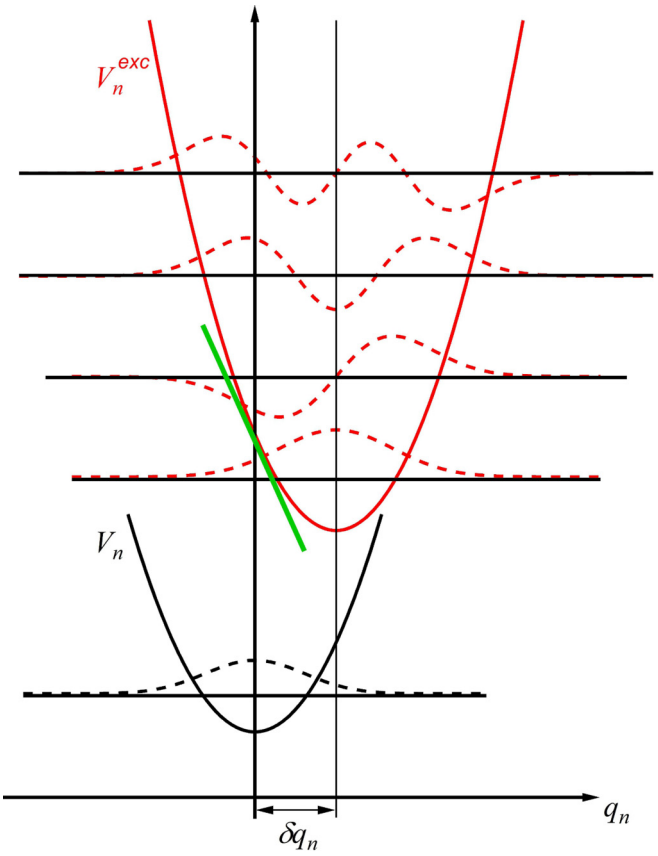

FIG. 11. Initial-state (black) and excited-state (red line) potential and wave functions. The gradient of the excited-state potential V_n^{exc} at $q_n = 0$ is indicated by a green line.

part of the spectra:

$$\delta q_n = \frac{1}{\omega_n^2}\left(\frac{\partial V_n^{exc}}{\partial q_n}\right)_{q_n=0}. \tag{2}$$

Combining (1) and (2), S_n can be expressed as

$$S_n = \frac{1}{2\hbar\omega_n^3}\left(\frac{\partial V_n^{exc}}{\partial q_n}\right)^2_{q_n=0} \tag{3}$$

Using the transformation to dimensionless normal coordinates $q_n \rightarrow \sqrt{\hbar/\omega_n}Q_n$, S_n simplifies to

$$S_n = \frac{1}{2}\frac{1}{(\hbar\omega_n)^2}\left(\frac{\partial V_n^{exc}}{\partial Q_n}\right)^2_{Q_n=0}. \tag{4}$$

This permits us to express the gradient of the excited potential in dimensionless normal coordinates directly in terms of the HR parameter:

$$g_n = \left(\frac{\partial V_n^{exc}}{\partial Q_n}\right)_{Q_n=0} = \hbar\omega_n\sqrt{2S_n}. \tag{5}$$

In adiabatic EPC systems, where electron dynamics is much faster than phonon dynamics ($\omega_{el} \gg \omega_n$), the dimensionless EPC constant λ_n is defined, through BCS-type theory, as

$$\lambda_n = \frac{g_n^2}{\hbar\omega_n}\chi(0) \tag{6}$$

where $\chi(0)$ is the electron-hole response function. Actually, the variation of atomic distances due to the excitation of mode n induces a modulation of electronic transfer integrals inside the system under consideration, here the $Cu_2(CN)_5H_4$ cluster. This stimulates additional charge transfer and electron-hole pair creation.

For an insulating system with a localized or negligibly dispersing (Einstein) phonon, the electron-hole response function at $q_n = 0$ and $\omega_n = 0$ can be derived in the frame of the dimer-charge oscillation model [39,40]:

$$\chi(0) = \sum_{i,j}\frac{|\langle i|\hat{o}|j\rangle|^2}{\hbar\omega_{i,j}}, \tag{7}$$

where the sum is performed over all possible electronic transitions from the occupied state i to the unoccupied state j, which are susceptible to being involved with the excitation of the phonon n. Supposing that the matrix elements of relevant processes are close to unity and all others are close to zero, $\chi(0)$ simplifies to

$$\chi(0) = \frac{\mathcal{N}}{\hbar\omega_{CT}}, \tag{8}$$

with $\mathcal{N}$ being the number of electronic transitions with energy $\hbar\omega_{CT}$ which participate in the EPC.

A cyanide group phonon in k-ET-Cu modulates electronic transfer integrals inside the anion layer as well as between the anion and cation layers. The two lowest-energy electronic excitations in the cluster are chosen as charge-transfer excitations which are related to the modulation of intralayer and interlayer electronic transfer integrals: $\pi_\perp \rightarrow \pi_\perp^*$ and $\pi_\parallel \rightarrow \pi_\perp^*$. The value of $\mathcal{N}$ is thus 2, and the expression of λ_n becomes

$$\lambda_a = \frac{2g_n^2}{(\hbar\omega_n)(\hbar\omega_{CT})}, \tag{9}$$

where $\hbar\omega_{CT}$ corresponds to the minimal charge-transfer excitation energy. It can be estimated from the calculation of the inelastic part of the spectra, in particular the energy of the $\pi_\parallel \rightarrow \pi_\perp^*$ and $\pi_\perp \rightarrow \pi_\perp^*$ excitations (structure A). The former is an in-plane charge transfer, and the latter is possibly involved in the interaction with the ET molecular layer. For the estimation of $\hbar\omega_{CT}$ we took the value from the calculated spectra with detuning $\Omega = -0.4$ eV, shown in Fig. 9. The value of $\hbar\omega_{CT} = 5$ eV corresponds to the energy loss of structure A, i.e., its position relative to the elastic peak, while its half width at half maximum is taken as the uncertainty $\Delta\hbar\omega_{CT} = 0.5$ eV. Taking this value into account, for the CN stretching mode ($h\omega_1 = 280$ meV), with HR parameter $S_1 = 0.334$ and $g_1 = 230$ meV, we estimate the value of the dimensionless EPC parameter to be $\lambda_1 = 0.076$.

Table II shows the dimensionless EPC parameters of all the anion plane modes strongly excited by the N K-edge RIXS process. They are individually lower than 0.08, but their total $\lambda_{\text{anion}} \approx 0.1$.

It is noteworthy that from IR and Raman measurements [40] the anion plane modes are considered to have negligible λ in the sister compound κ-$(ET)_2Cu(SCN)_2$. The same measurements reveal that the ET molecular CC stretching mode is strongly coupled with $\lambda_{CC} = 0.17$. Similar measurements on β-$(ET)_2I_3$

estimate the total ET molecular layer contribution to the EPC is $\lambda_{ET} \approx 0.4$ [41]. Our estimation of the EPC in κ-$(ET)_2Cu_2(CN)_3$ shows that the coupling of the anion modes is certainly not negligible. Their contribution to the total λ is at least 20%.

Although the anion-donor coupling is not included in the present calculation, it is important to realize that the nitrogen displacement induces two types of indirect effects on the electronic structure of the ET layer. First, it tilts the H bond, inducing (small) displacements of the ET molecule, which modulates the inter-ET transfer integrals. Second, it varies the H-bond distance and induces the H-bond polarization effect, which modulates inner σ electron density of the occupied levels of the ET molecule [14]. This intramolecular electron transfer induces a modulation of the π-hole density on the core of the ET molecules. A similar charge modulation process was previously invoked as a consequence of the establishment of H bonds accompanying the charge ordering transition in several families of ET salts [14,15].

Our data show that the EPC of N_C sites, more strongly H bonded to the ET-ethylene end groups, involves almost solely the CN stretching motion. In addition, the EPC of the N_B sites involves all cluster CN modes depicted in Fig. 4. This complex dynamics, together with the orientational disorder of CN_B cyanides, creates a substantially disordered environment of each ET molecule, which is both static and dynamic. The observation of the near-neighbor and variable-range hopping mechanisms of conductivity [16,17] and the glassy behavior in dielectric spectroscopy [16] indicate that such a disorder is certainly relevant. We note that charge degrees of freedom play an important role in the physics of k-ET-Cu, meaning that one should go beyond the simple spin-liquid description originally considered [4], which takes into account only magnetic frustration between localized spins.

VII. CONCLUSION

We showed that the N K-edge RIXS permits us to clearly observe up to five lattice vibration harmonics of selected modes in the κ-(BEDT-TTF)$_2$Cu$_2$(CN)$_3$ spin-liquid insulator. Tuning the incoming photon energy to the K edge of two nonequivalent N sites switches on different sets of phonon modes. The CN stretching mode is strongly excited at the edge of the ordered nitrogen sites which are more strongly connected to the BEDT-TTF molecules ($h\nu = 399.8$ eV), while positionally disordered sites show multimode excitation ($h\nu = 398.4$ eV). The difference in their resonant energy $h\nu$ demonstrates that their environment alters the electronic state, while the complete change in their vibrational progression points to the degree of preventing the mechanical movement. RIXS spectra are reproduced by calculations on a $Cu_2(CN)_5H_4$ cluster cut from the anion plane and terminated by H atoms. They permit us to estimate that the contribution of the anion plane modes to the total dimensionless electron-phonon coupling parameter of the κ-(BEDT-TTF)$_2$Cu$_2$(CN)$_3$ compound is about 20%.

ACKNOWLEDGMENTS

S.T. acknowledges the support of the Croatian Science Foundation under the Project IP-2013-11-1011. P.L. was supported by the Unity Through Knowledge Fund, Contract No. 22/15 and H2020 CSA Twinning Project No. 692194, RBI-T-WINNING. K.M. and K.K. acknowledge the support of Japan Society for the Promotion of Science (JSPS) KAKENHI under Grants No. 25220709 and No. 17K05532.

[1] F. Giustino, Rev. Mod. Phys. **89**, 015003 (2017).
[2] B. Mansart, D. Boschetto, A. Savoia, F. Rullier-Albenque, F. Bouquet, E. Papalazarou, A. Forget, D. Colson, A. Rousse, and M. Marsi, Phys. Rev. B **82**, 024513 (2010).
[3] L. Chaix, G. Ghiringhelli, Y. Y. Peng, M. Hashimoto, B. Moritz, K. Kummer, N. B. Brookes, Y. He, S. Chen, S. Ishida, Y. Yoshida, H. Eisaki, M. Salluzzo, L. Braicovich, Z.-X. Shen, T. P. Devereaux, and W.-S. Lee, Nat. Phys. **13**, 952 (2017).
[4] Y. Shimizu, K. Miyagawa, K. Kanoda, M. Maesato, and G. Saito, Phys. Rev. Lett. **91**, 107001 (2003).
[5] U. Geiser, H. H. Wang, K. D. Carlson, J. M. Williams, H. A. Charlier, Jr., J. E. Heindl, G. A. Yaconi, B. J. Love, M. W. Lathrop, J. E. Schirber, D. L. Overmyer, J. Ren, and M.-H. Whangbo, Inorg. Chem. **30**, 2586 (1991).
[6] T. Komatsu, N. Matsukawa, T. Inoue, and G. Saito, J. Phys. Soc. Jpn. **65**, 1340 (1996).
[7] Y. Kurosaki, Y. Shimizu, K. Miyagawa, K. Kanoda, and G. Saito, Phys. Rev. Lett. **95**, 177001 (2005).
[8] H. C. Kandpal, I. Opahle, Y.-Z. Zhang, H. O. Jeschke, and R. Valenti, Phys. Rev. Lett. **103**, 067004 (2009).
[9] H. O. Jeschke, M. de Souza, R. Valenti, R. S. Manna, M. Lang, and J. A. Schlueter, Phys. Rev. B **85**, 035125 (2012).
[10] C. Hotta, Phys. Rev. B **82**, 241104 (2010).
[11] S. Ishihara, J. Phys. Soc. Jpn. **79**, 011010 (2010).
[12] M. Poirier, M. de Lafontaine, K. Miyagawa, K. Kanoda, and Y. Shimizu, Phys. Rev. B **89**, 045138 (2014).
[13] F. Kagawa, K. Miyagawa, and K. Kanoda, Nature (London) **436**, 534 (2005).
[14] P. Alemany, J.-P. Pouget, and E. Canadell, Phys. Rev. B **85**, 195118 (2012).
[15] P. Alemany, J.-P. Pouget, and E. Canadell, J. Phys.: Condens. Matter **27**, 465702 (2015).
[16] M. Pinteric, M. Čulo, O. Milat, M. Basletić, B. Korin-Hamzić, E. Tafra, A. Hamzić, T. Ivek, T. Peterseim, K. Miyagawa, K. Kanoda, J. A. Schlueter, M. Dressel, and S. Tomić, Phys. Rev. B **90**, 195139 (2014).
[17] M. Čulo, E. Tafra, M. Basletić, S. Tomić, A. Hamzić, B. Korin-Hamzić, M. Dressel, and J. A. Schlueter, Phys. B (Amsterdam, Neth.) **460**, 208 (2015).
[18] K. Sedlmeier, S. Elsässer, D. Neubauer, R. Beyer, D. Wu, T. Ivek, S. Tomić, J. A. Schlueter, and M. Dressel, Phys. Rev. B **86**, 245103 (2012).
[19] M. Abdel-Jawad, I. Terasaki, T. Sasaki, N. Yoneyama, N. Kobayashi, Y. Uesu, and C. Hotta, Phys. Rev. B **82**, 125119 (2010).
[20] M. Sacchi, N. Jaouen, H. Popescu, R. Gaudemer, J. M. Tonnerre, S. G. Chiuzbăian, C. F. Hague, A. Delmotte, J. M. Dubuisson, G. Cauchon, B. Lagarde, and F. Polack, J. Phys.: Conf. Ser. **425**, 072018 (2013).

[21] S. G. Chiuzbăian, C. F. Hague, A. Avila, R. Delaunay, N. Jaouen, M. Sacchi, F. Polack, M. Thomasset, B. Lagarde, A. Nicolaou, S. Brignolo, C. Baumier, J. Lüning, and J.-M. Mariot, Rev. Sci. Instrum. **85**, 043108 (2014).

[22] O. Bunau and Y. Joly, J. Phys.: Condens. Matter **21**, 345501 (2009).

[23] S. A. Guda, A. A. Guda, M. A. Soldatov, K. A. Lomachenko, A. L. Bugaev, C. Lamberti, W. Gawelda, C. Bressler, G. Smolentsev, A. V. Soldatov, and Y. Joly, J. Chem. Theory Comput. **11**, 4512 (2015).

[24] M. W. Schmidt, K. K. Baldridge, J. A. Boatz, S. T. Elbert, M. S. Gordon, J. H. Jensen, S. Koseki, N. Matsunaga, K. A. Nguyen, S. Su, T. L. Windus, M. Dupuis, and J. A. Montgomery, Jr., J. Comput. Chem. **14**, 1347 (1993).

[25] T. Darrah Thomas, L. J. Saethre, S. L. Sorensen, and S. Svensson, J. Chem. Phys. **109**, 1041 (1998).

[26] S. Carniato, V. Ilakovac, J.-J. Gallet, E. Kukk, and Y. Luo, Phys. Rev. A **70**, 032510 (2004).

[27] S. Carniato, V. Ilakovac, J.-J. Gallet, E. Kukk, and Y. Luo, Phys. Rev. A **71**, 022511 (2005).

[28] V. Ilakovac, S. Carniato, J.-J. Gallet, E. Kukk, D. Horvatić, and A. Ilakovac, Phys. Rev. A **77**, 012516 (2008).

[29] V. Ilakovac, Y. Houari, S. Carniato, J.-J. Gallet, E. Kukk, and D. Horvatić, Phys. Rev. A **85**, 062521 (2012).

[30] M. Dressel, P. Lazić, A. Pustogow, E. Zhukova, B. Gorshunov, J. A. Schlueter, O. Milat, B. Gumhalter, and S. Tomić, Phys. Rev. B **93**, 081201(R) (2016).

[31] The standard error of DFT-based calculations of vibrations is taken as the uncertainty of the wave numbers $\Delta\sigma_n$ (and thus energy quanta $\Delta\hbar\omega_n$) of each mode. ΔS_n (Δg_n) is derived from the error of the relative shift of the excited- and initial-state potentials. $\Delta\lambda_n$ includes, besides Δg_n and $\Delta\hbar\omega_n$, $\Delta\hbar\omega_{CT}$, as explained in the Sec. VI.

[32] M. Simon, L. Journel, R. Guillemin, W. C. Stolte, I. Minkov, F. Gel'mukhanov, P. Sałek, H. Ågren, S. Carniato, R. Taïeb, A. C. Hudson, and D. W. Lindle, Phys. Rev. A **73**, 020706 (2006).

[33] J. L. Ament, M. van Veenendaal, and J. van den Brink, Europhys. Lett. **95**, 27008 (2011).

[34] S. Moser, S. Fatale, P. Krüger, H. Berger, P. Bugnon, A. Magrez, H. Niwa, J. Miyawaki, Y. Harada, and M. Grioni, Phys. Rev. Lett. **115**, 096404 (2015).

[35] S. Fatale, S. Moser, J. Miyawaki, Y. Harada, and M. Grioni, Phys. Rev. B **94**, 195131 (2016).

[36] J. L. Campbell and T. Papp, At. Data Nucl. Data Tables **77**, 1 (2001).

[37] M. Neeb, J.-E. Rubensson, M. Biermann, and W. Eberhardt, J. Electron Spectrosc. **67**, 261 (1994).

[38] K. Huang and A. Rhys, Proc. R. Soc. London, Ser. A **204**, 406 (1950).

[39] M. J. Rice, Solid State Commun. **31**, 93 (1979).

[40] R. D. McDonald, A.-K. Klehe, J. Singleton, and W. Hayes, J. Phys.: Condens. Matter **15**, 5315 (2003).

[41] A. Girlando, M. Masino, G. Visentini, R. G. Della Valle, A. Brillante, and E. Venuti, Phys. Rev. B **62**, 14476 (2000).